ChemComm

Single crystal growth and magnetic properties of the mixed valent Yb containing Zintl phase, Yb14MgSb11

Journal:	*ChemComm*
Manuscript ID	CC-COM-07-2018-005471.R2
Article Type:	Communication

Journal Name

COMMUNICATION

Single crystal growth and magnetic properties of the mixed valent Yb containing Zintl phase, $Yb_{14}MgSb_{11}$

Received 00th January 20xx,
Accepted 00th January 20xx

DOI: 10.1039/x0xx00000x

www.rsc.org/

Elizabeth L. Kunz Wille[a] , Na Hyun Jo[b] , James C. Fettinger[a], Paul C. Canfield[b] and Susan M. Kauzlarich*[a]

Large crystals of $Yb_{14}MgSb_{11}$ were grown through a Sn flux method. Magnetic Susceptibility measurements yield an effective magnetic moment of 3.4(1) μ_B, revealing the presence of both divalent and trivalent Yb in $Yb_{14}MgSb_{11}$. Previously assumed to only contain Yb^{2+} as in $Yb_{14}MnSb_{11}$, the mixed valency demonstrates that $Yb_{14}MgSb_{11}$ is a Zintl phase.

Zintl phase compounds have been under investigation as thermoelectric materials since the discovery of the high zT of $Yb_{14}MnSb_{11}$.[1] Zintl phases are considered to be valence-precise, with donation of electrons from the electropositive elements to the more electronegative, and the electronegative elements satisfying their valence via bonding.[2] In the same structure type, many different elements can be substituted, and strategic employment of atoms of different electronegativities can result in subtle electronic tuning which is crucial for optimizing the thermoelectric figure of merit, *zT*. $zT = \alpha^2 T/\rho\kappa$, where α is the Seebeck coefficient, ρ the electrical resistivity and κ the thermal conductivity. These properties are inter-related through carrier concentration, making optimization of a TE material a synthetic challenge.[3] The optimal carrier concentration for the maximization of *zT* is typically between 10^{19} and 10^{21} cm^{-3}.[4] $Yb_{14}MgSb_{11}$ is a compound of the 14-1-11 family (Figure 1) and is of interest for thermoelectric (TE) applications and possesses a high *zT* similar to that of $Yb_{14}MnSb_{11}$, the current state of the art high temperature p-type TE material.[1] Additionally, $Yb_{14}MgSb_{11}$ exhibits lower sublimation and lower carrier concentration than $Yb_{14}MnSb_{11}$, which results in an improved Seebeck coefficient.[5] $Yb_{14}MnSb_{11}$ has a reported room temperature carrier concentration of 1.3 x 10^{21} cm^{-3},[6] and $Yb_{14}MgSb_{11}$, 3.7 x 10^{20} cm^{-3}.[5] Figure 1 shows the crystal structure of $Yb_{14}MgSb_{11}$ viewed down the *c* axis. $Yb_{14}MnSb_{11}$, has been shown to contain only Yb^{2+} through thermodynamic measurements,[7] X-Ray Photoelectron Spectroscopy (XPS) and X-ray magnetic circular dichroism (XMCD) measurements.[8, 9] Studies of $Yb_{14}MnSb_{11}$ with small amounts of 3+ rare earth element substitution have been investigated, resulting in reduction of the carrier concentration, and thus improvement of *zT*.[10-14] A limit of 0.7 > x has been found for these $Yb_{14-x}RE_xMnSb_{11}$ compounds.

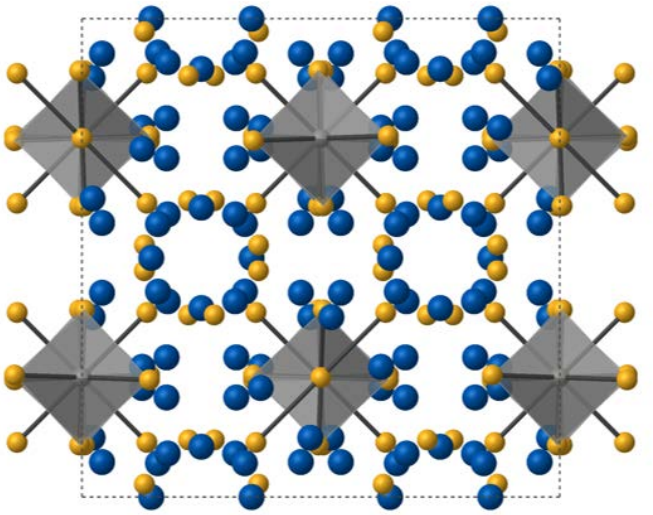

Figure 1. A view down the *c* axis of $Yb_{14}MgSb_{11}$ (tetragonal, $I4_1/acd$). The Yb atoms are shown in blue, Sb in gold, and the grey tetrahedra are $MgSb_4$.

It was speculated that $Yb_{14}MgSb_{11}$ would contain only Yb^{2+}, similar to $Yb_{14}MnSb_{11}$, and that the lack of *d* electrons and changes to the size of the unit cell along with the changes in the tetrahedral site geometry might be responsible for its lowered carrier concentration.[5, 15] However, it is possible that mixed valence of Yb, similar to that observed in $Yb_{14}ZnSb_{11}$, could contribute to the lowered carrier concentration.[5] The isostructural $Yb_{14}ZnSb_{11}$ is more metallic than $Yb_{14}MnSb_{11}$ and contains both Yb^{2+} and Yb^{3+}.[15] $Yb_{14}ZnSb_{11}$ shows a magnetic

[a] Address here. Department of Chemistry, University of California, Davis, One Shields Avenue, Davis, CA 95616
[b] Ames Laboratory US DOE and Department of Physics and Astronomy, Iowa State University, Ames IA 50011
† Electronic Supplementary Information (ESI) available: experimental methods, CIF. See DOI: 10.1039/x0xx00000x

transition attributed to a valence fluctuation of Yb^{3+} to Yb^{2+} at 85 K.[15] XPS measurements verified the presence of Yb^{3+} in $Yb_{14}ZnSb_{11}$, and its metallic behavior is attributed to a shift of the Yb 4f levels due to this mixed valency.[8]

$Yb_{14}MgSb_{11}$ has been reported in literature, prepared from the stoichiometric reaction of the elements with Mg is excess (prepared from a molar ratio of 14 Yb: 2 Mg: 11 Sb annealed in a sealed Nb tube at 1000°C for 12 days) which resulted in small crystals unsuitable for magnetic susceptibility measurements.[5] The $A_{14}MgSb_{11}$ (A= Ca[5], Eu, Sr[16]) and $A_{14}MgBi_{11}$ (A= Ca, Sr, Eu[17], Yb[18]) analogs all have similar reported syntheses in either Ta or Nb tubes, with anneal temperatures ranging from 950-1100°C. In contrast, solution growth of crystals can often result in large (some >100 mg), high quality samples and are ideal for magnetic measurements.[19, 20] The published optimized syntheses of large crystals of $Yb_{14}MnSb_{11}$ and $Yb_{14}ZnSb_{11}$ employ tin as the flux 'solvent' because Sn does not incorporate into the structure of the desired 14-1-11 phase at the dilutions used.[7, 15] The Sn-flux synthesis of $Yb_{14}ZnSb_{11}$ detailed by Fisher et al.[15] was used as a starting point in this work, with temperature profile considerations taken into account in order to accommodate the high vapour pressure of Mg (see †ESI). Vaporization of Mg is evident as a brown deposition inside the silica tube after the reaction is removed from the furnace. The ratio of Sn to Yb, Mg and Sb was increased in a complimentary effort to incorporate all elements into the melt at the lower temperatures used. Optimization of these parameters limited the formation of unwanted side products such as Yb_5Sb_3 and $Yb_{11}Sb_{10}$. Fritted alumina crucible sets[21] were used and aid in the production of large crystals. Crystals of $Yb_{14}MgSb_{11}$ obtained from this optimized flux synthesis were shiny, faceted and could be clearly identified by their geometry. Figure 2 is a photograph of one such crystal obtained from this optimized synthesis.

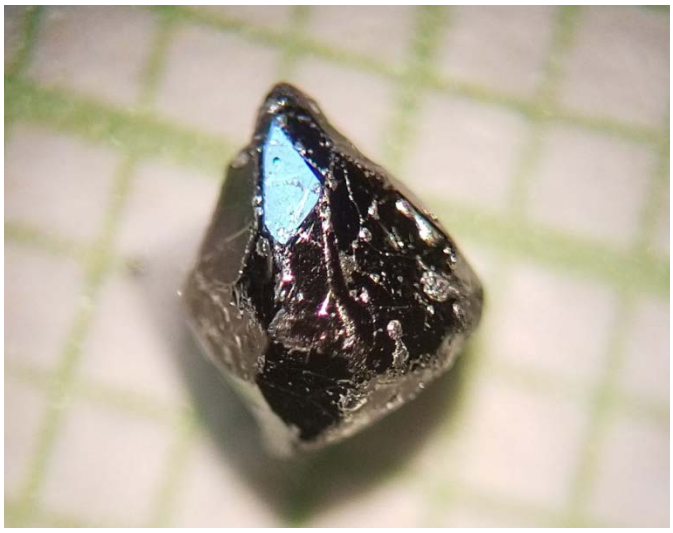

Figure 2. A solution-grown crystal of $Yb_{14}MgSb_{11}$. Background grid is $1mm^2$. Some surface Sn is present.

Single crystal data and refinement information is detailed in Table 1. $Yb_{14}MgSb_{11}$ crystallizes in the *I4₁/acd* space group and one formula unit can be described as containing a tetrahedral $(MgSb_4)^{10-}$ unit, a linear $(Sb_3)^{7-}$ unit and isolated Sb^{3-} anions, along with Yb cations. Table 2 summarizes results from flux grown single crystals of previously reported $Yb_{14}MnSb_{11}$ and $Yb_{14}ZnSb_{11}$ and compares them to this work. Notably, for the Mg analogue, the *c*/*a* ratio is larger and the angles are closer to the tetrahedral ideal. $Yb_{14}MgSb_{11}$ has a less compressed M-Sb_4 tetrahedron, a longer M-Sb bond and larger lattice parameters than those of Zn and Mn. The 4 Yb sites in $Yb_{14}MSb_{11}$ are often compared by the volume of the polyhedron between each Yb and its nearest neighbour Sb atoms.[12, 22] Figure 3 shows the Yb site polyhedral volumes for the Mg, Mn, and Zn analogs. $Yb_{14}MgSb_{11}$ exhibits the largest volumes for each cation site, with Yb4 showing the largest volume difference between Mg and its Mn and Zn counterparts. In RE^{3+} substituted systems of $Yb_{14}MnSb_{11}$, site specificity is often seen depending on the size of the substituted atom. Larger RE atoms such as Ce^{3+} substitute on the Yb2 and Yb4 sites,[12] while much smaller atoms such as Sc^{3+} substitute on the Yb1 and Yb3 sites,[13] and mid-size atoms such as Y^{3+} substitute across all Yb sites.[13] While Yb3 has a large volume, it is the least distorted octahedron of all the cation sites. A refinement allowing Mg to occupy the Yb1 and Yb3 sites resulted in a *GooF* of 1.22 and *R1*/*wR2* values of 0.0205/0.0246. Mg^{2+} preferentially occupying the Yb1 and Yb3 sites in $Yb_{14}MgSb_{11}$ is consistent with the behavior of similarly sized cations such as Sc^{3+}. This result is consistent with the unit cell volume being about 65 $Å^3$ smaller than that obtained from non-solution grown crystals in prior work.[5]

Table 1. Data collection and refinement parameters

	$Yb_{14}MgSb_{11}$
formula unit	$Yb_{13.85}Mg_{1.15}Sb_{11}$
crystal system	tetragonal
space group	*I4₁/acd* (no. 142)
molar mass	3742.43 g/mol
T	100(2) K
Z	8
radiation	Mo Kα, λ = 0.71073Å
ρ_{calc}	8.18 g/cm³
a	16.566(2) Å
c	22.151(2) Å
Volume	6079(2) Å³
abs. coeff. μ	51.28 mm^{-1}
reflns/indep. reflns	31164/2224
parameters refined	64
GooF	1.224
***R1* (all)**	0.0205
***wR2* (all)**	0.0246

Table 2. Lattice parameters and selected bond distances and angles for $Yb_{14}MSb_{11}$ (M = Mg, Mn, Zn)

	$Yb_{14}MgSb_{11}$	$Yb_{14}MnSb_{11}$[11]	$Yb_{14}ZnSb_{11}$[8]
***a* (Å)**	16.566(2)	16.586(2)	16.562(3)
***c* (Å)**	22.151(2)	21.911(2)	21.859(2)
V (Å³)	6079(2)	6027.5(9)	5995.9(2)
***c*/*a* ratio**	1.337(2)	1.321(2)	1.319(3)

MSb_4 tetrahedron angles (°)	106.78(2) 114.99(2)	105.56(2) 117.61(2)	105.59(2) 117.56(2)
M-Sb bond length (Å)	2.7949(5)	2.7435(7)	2.7255(8)

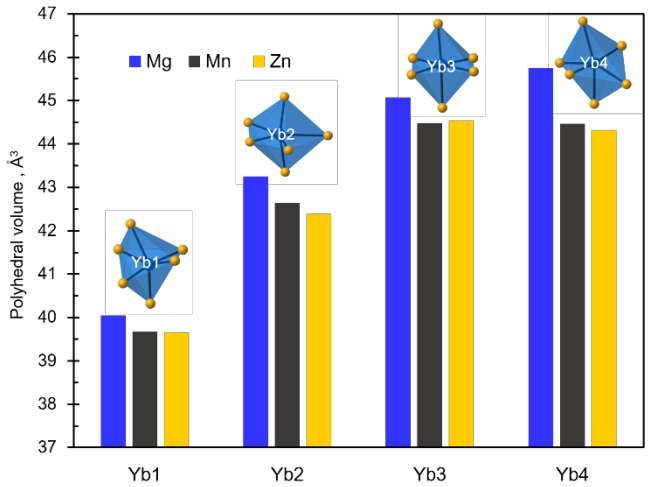

Figure 3. Polyhedral volume of the Yb cations for $Yb_{14}MSb_{11}$ (M = Mg[5], Mn[11], Zn[8]).

Electron microprobe analysis was used to produce backscatter images and X-Ray maps of a polished crystal of $Yb_{14}MgSb_{11}$ are provided in Figure 4. Wavelength dispersive spectroscopy (WDS) was used to quantify elemental ratios, and the composition of $Yb_{13.7(2)}Mg_{1.20(4)}Sb_{11.00(9)}$ was obtained. Substitution of small amounts of Mg on the Yb site is consistent with the composition from WDS. A more accurate manner of writing the formula of this compound is $(Yb_{13.8}Mg_{0.2})MgSb_{11}$.

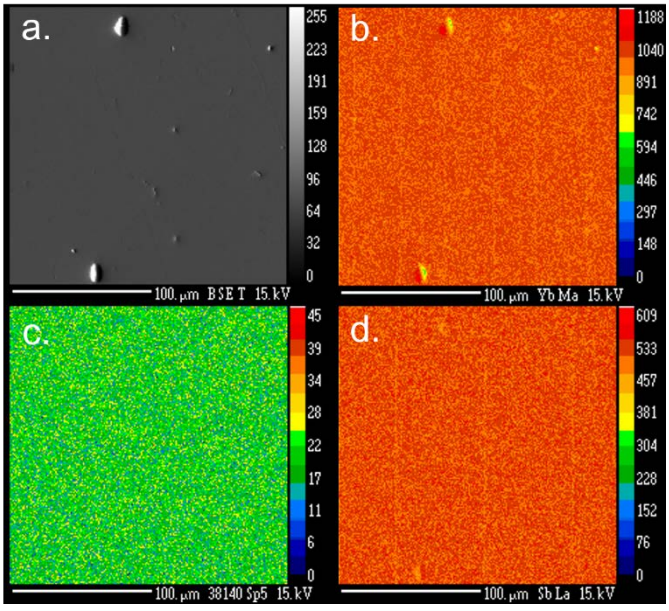

Figure 4. Electron microprobe (a) back scattered topological image and X-ray elemental maps of (b) Yb Mα, (c) Mg Kα, and (d) Sb Lα.

Magnetic susceptibility was measured on crystals cleaned of surface Sn flux from 2K to 300K with a field of 1 T and is shown in Figure 5. The plot of $1/\chi$ vs T is linear and was fit using the paramagnetic Curie-Weiss law, $\chi(T) = C/(T-\theta)$, where C is the Curie constant and ϑ the Weiss temperature. A linear fit of this data from 250 K to 50 K yielded a Curie constant of 1.46(3) and a Weiss constant of 3.6(2) K. The effective magnetic moment was calculated from $\mu_{eff} = 2.82\sqrt{C}$ and found to be 3.4(1) μ_B per formula unit. Yb^{3+} has a single unpaired electron and possesses an effective magnetic moment of 4.5 μ_B, while all other constituents of this compound contain no unpaired electrons that could contribute to this signal.

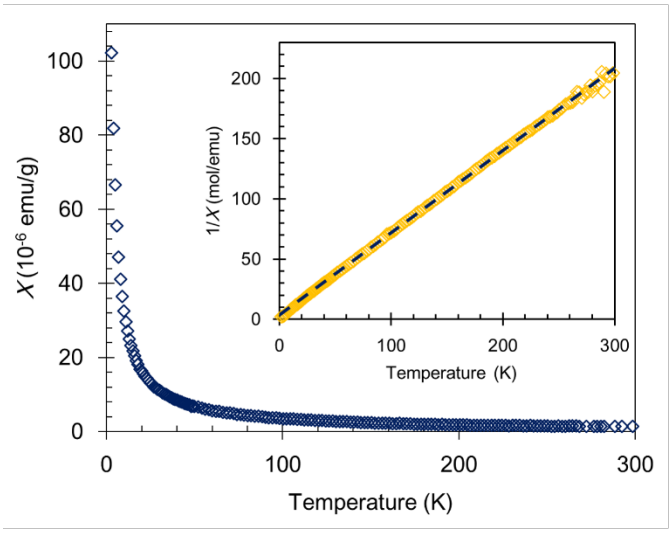

Figure 5 Magnetic susceptibility (emu/gm) as a function of temperature (K), measured at 1 T for $Yb_{14}MgSb_{11}$. The inset shows the inverse of the susceptibility (mol/emu) vs temperature (K).

The value of 3.4(1) μ_B per formula unit suggests that there is trivalent Yb present in $Yb_{14}MgSb_{11}$ and provides a good justification for the observed lower carrier concentration compared with that of $Yb_{14}MnSb_{11}$. Normalizing for unit cell volume, the difference between $Yb_{14}MnSb_{11}$ and $Yb_{14}MgSb_{11}$ is 5.6 carriers using $N = V*n$, where V is the unit cell volume and n is the carrier concentration. It is apparent that the previous speculation of a change in unit cell volume cannot account for this difference. This value is close, however, to the number of carriers calculated for the addition of 0.76 Yb^{3+} per formula unit to the system, 6.1 carriers, consistent with the presence of Yb^{3+}. $Yb_{14}ZnSb_{11}$ also shows the presence of Yb^{3+} but there is a transition to Yb^{2+} at low temperature. $Yb_{14}ZnSb_{11}$ follows Curie-Weiss temperature-dependent behaviour and has an effective magnetic moment of 3.8(1) μ_B above 150 K.[15] Around 85 K, a broad maximum in the susceptibility is reached and a decrease is observed and was attributed to a valence fluctuation of Yb. Interestingly, this valence fluctuation exhibited by $Yb_{14}ZnSb_{11}$ is not evident in the susceptibility measurement of $Yb_{14}MgSb_{11}$. Valence fluctuations have been observed at low temperatures in other Yb containing compounds [23] and it has been suggested that it is indicative of a hybridization of 4*f* states and conduction electrons.[24, 25] In the case of $Yb_{14}MgSb_{11}$, the carrier concentration is significantly lower than that of the Zn analog and there is no evidence for valence fluctuations in the

magnetic data down to 2 K. $Yb_{14}MgSb_{11}$ can be considered almost a Zintl phase where 0.76 Yb^{3+} provides the additional 0.76 electron, very close to the total of 1 electron necessary to be an electron precise semiconductor: $13(Yb^{2+}/Mg^{2+}) + 1Yb^{3+} + MgSb_4^{10-} + Sb_3^{7-} + 4Sb^{3-}$. The variation in Yb valence across these compounds, Mg, Mn, and Zn analogs, indicates a rich chemistry with opportunities for unique magnetic and electronic properties.

Financial support for E.K.W. from the Nuclear Energy University Program (NEUP) is gratefully acknowledged. This work was supported by the U.S. Department of Energy, Office of Science, Office of Workforce Development for Teachers and Scientists, Office of Science Graduate Student Research (SCGSR) program. The SCGSR program is administered by Oak Ridge Institute for Science and Education for the DOE under contract DE-SC0014664. Work at Ames Lab (P. C. C. and N-H. J.) was supported by the U.S. Department of Energy, Office of Basic Energy Science, Division of Materials Sciences and Engineering. Ames Laboratory is operated for the U.S. Department of Energy by Iowa State University under Contract No. DE-AC02-07CH11358. N-H. J. was funded by the Gordon and Betty Moore Foundation's EPiQS Initiative through Grant GBMF4411. Mr. Nick Botto of the UCD Geology Department is thankfully acknowledged for electron microprobe/WDS measurements.

Conflicts of interest

There are no conflicts to declare.

Notes and references

1 S. R. Brown, S. M. Kauzlarich, F. Gascoin and G. J. Snyder, *Chemistry of Materials*, 2006, **18**, 1873-1877.
2 S. M. Kauzlarich, S. R. Brown and G. Jeffrey Snyder, *Dalton Transactions*, 2007, DOI: 10.1039/B702266B, 2099-2107.
3 X. Zhang and L.-D. Zhao, *Journal of Materiomics*, 2015, **1**, 92-105.
4 G. J. Snyder and E. S. Toberer, *Nat Mater*, 2008, **7**, 105-114.
5 Y. Hu, J. Wang, A. Kawamura, K. Kovnir and S. M. Kauzlarich, *Chemistry of Materials*, 2015, **27**, 343-351.
6 S. Toberer Eric, A. Cox Catherine, R. Brown Shawna, T. Ikeda, F. May Andrew, M. Kauzlarich Susan and G. J. Snyder, *Advanced Functional Materials*, 2008, **18**, 2795-2800.
7 I. R. Fisher, T. A. Wiener, S. L. Bud'ko, P. C. Canfield, J. Y. Chan and S. M. Kauzlarich, *Physical Review B*, 1999, **59**, 13829-13834.
8 A. P. Holm, T. C. Ozawa, S. M. Kauzlarich, S. A. Morton, G. Dan Waddill and J. G. Tobin, *Journal of Solid State Chemistry*, 2005, **178**, 262-269.
9 A. P. Holm, S. M. Kauzlarich, S. A. Morton, G. D. Waddill, W. E. Pickett and J. G. Tobin, *Journal of the American Chemical Society*, 2002, **124**, 9894-9898.
10 Y. Hu, S. K. Bux, J. H. Grebenkemper and S. M. Kauzlarich, *Journal of Materials Chemistry C*, 2015, **3**, 10566-10573.
11 J. H. Roudebush, J. Grebenkemper, Y. Hu, N. Kazem, M. N. Abdusalyamova and S. M. Kauzlarich, *Journal of Solid State Chemistry*, 2014, **211**, 206-211.
12 J. H. Grebenkemper and S. M. Kauzlarich, *APL Materials* 2015, **3**, 041503.
13 J. H. Grebenkemper, S. Klemenz, B. Albert, S. K. Bux and S. M. Kauzlarich, *Journal of Solid State Chemistry*, 2016, **242**, 55-61.
14 Y. Hu, C.-W. Chen, H. Cao, F. Makhmudov, J. H. Grebenkemper, M. N. Abdusalyamova, E. Morosan and S. M. Kauzlarich, *Journal of the American Chemical Society*, 2016, **138**, 12422-12431.
15 I. R. Fisher, S. L. Bud'ko, C. Song, P. C. Canfield, T. C. Ozawa and S. M. Kauzlarich, *Physical Review Letters*, 2000, **85**, 1120-1123.
16 W.-j. Tan, Y.-t. Liu, M. Zhu, T.-j. Zhu, X.-b. Zhao, X.-t. Tao and S.-q. Xia, *Inorganic Chemistry*, 2017, **56**, 1646-1654.
17 W. Tan, Z. Wu, M. Zhu, J. Shen, T. Zhu, X. Zhao, B. Huang, X.-t. Tao and S.-q. Xia, *Inorganic Chemistry*, 2017, **56**, 10576-10583.
18 Y. Hu and S. M. Kauzlarich, *Dalton Transactions*, 2017, **46**, 3996-4003.
19 P. C. Canfield and Z. Fisk, *Philosophical Magazine Part B*, 1992, **65**, 1117-1123.
20 I. R. Fisher, M. C. Shapiro and J. G. Analytis, *Philosophical Magazine*, 2012, **92**, 2401-2435.
21 P. C. Canfield, T. Kong, U. S. Kaluarachchi and N. H. Jo, *Philosophical Magazine*, 2016, **96**, 84-92.
22 I. G. Vasilyeva, R. E. Nikolaev, M. N. Abdusaljamova and S. M. Kauzlarich, *Journal of Materials Chemistry C*, 2016, **4**, 3342-3348.
23 D. T. Adroja, S. K. Malik, B. D. Padalia, S. N. Bhatia, R. Walia and R. Vijayaraghavan, *Physical Review B*, 1990, **42**, 2700-2703.
24 S. Chatterjee, J. P. Ruf, H. I. Wei, K. D. Finkelstein, D. G. Schlom and K. M. Shen, *Nature Communications*, 2017, **8**, 852.
25 M. Okawa, M. Matsunami, K. Ishizaka, R. Eguchi, M. Taguchi, A. Chainani, Y. Takata, M. Yabashi, K. Tamasaku, Y. Nishino, T. Ishikawa, K. Kuga, N. Horie, S. Nakatsuji and S. Shin, *Physical Review Letters*, 2010, **104**, 247201.

TOC: Large crystals of $Yb_{14}MgSb_{11}$ prepared by Sn flux show the presence of Yb^{3+} making this compound a Zintl phase.